

Contribution of Bistability and Noise to Cell Fate Transitions Determined by Feedback Opening

Chieh Hsu^{1,2,†}, Vincent Jaquet^{1,†}, Farzaneh Maleki¹ and Attila Becskei¹

¹ - Biozentrum, University of Basel, Klingelbergstrasse 50/70, 4056 Basel, Switzerland

² - School of Biosciences, University of Kent, Canterbury, Kent CT2 7NJ, UK

Correspondence to Attila Becskei: attila.becskei@unibas.ch

<http://dx.doi.org/10.1016/j.jmb.2016.07.024>

Edited by Sarah A. Teichmann

Abstract

Alternative cell fates represent a form of non-genetic diversity, which can promote adaptation and functional specialization. It is difficult to predict the rate of the transition between two cell fates due to the strong effect of noise on feedback loops and missing parameters. We opened synthetic positive feedback loops experimentally to obtain open-loop functions. These functions allowed us to identify a deterministic model of bistability by bypassing noise and the requirement to resolve individual processes in the loop. Combining the open-loop function with kinetic measurements and reintroducing the measured noise, we were able to predict the transition rates for the feedback systems without parameter tuning. Noise in gene expression was the key determinant of the transition rates inside the bistable range. Transitions between two cell fates were also observed outside of the bistable range, evidenced by bimodality and hysteresis. In this case, a slow transient process was the rate-limiting step in the transitions. Thus, feedback opening is an effective approach to identify the determinants of cell fate transitions and to predict their rates.

© 2016 The Authors. Published by Elsevier Ltd. This is an open access article under the CC BY-NC-ND license (<http://creativecommons.org/licenses/by-nc-nd/4.0/>).

Introduction

Genetically identical cells with two distinct phenotypes can coexist and persist in an identical environment, provided they were exposed to different conditions in the past and can display bistability. Bistability plays important roles in adaptation and cell differentiation in uni- and multicellular organisms. Typically, bistability arises due to positive feedback loops [1–3].

In a bistable feedback, a feedback component can have either low or high concentration in the steady state. Which state is reached depends only on the initial condition. If, initially, an external factor induces a cell to express a sufficiently high concentration of a component, the high expression will persist even after the factor is removed. Such a purely deterministic view of steady-state bistability needs to be modified in biological systems because transitions occur between two states. Transition rates can span a broad range; it is a rare event, for example, in the lysis–lysogeny cycle of the lambda phage. On the other hand, bacteria can switch to the competent form at high frequency [4,5]. The prediction of these

rates is crucial because they determine the proportion of the two cell types in a cell population and the efficiency of cellular reprogramming [6,7].

Typically, noise is considered a driving force of such transitions in genetic systems [8]. The interaction between a bistable system and noise is often conceptualized by depicting the deterministic bistable system by a potential landscape; the two stable states correspond to the two lowest points in the potential wells, which are separated by a barrier (Fig. 1a) [9]. When the system is exposed to noise, small fluctuations may not be sufficient to switch the cells to the other state, but larger fluctuations would do this (Fig. 1a, lower left panel). On the other hand, if the barrier is lower, even weak noise can switch the cells (Fig. 1a, lower right panel).

Thus, bistability amplifies the effect of noise; a sufficiently strong noise can induce most of the cells to switch to the higher state even though the deterministic description predicts the system to be at the low state. Consequently, the deterministic and stochastic descriptions of bistable systems are completely different [10], which makes the prediction

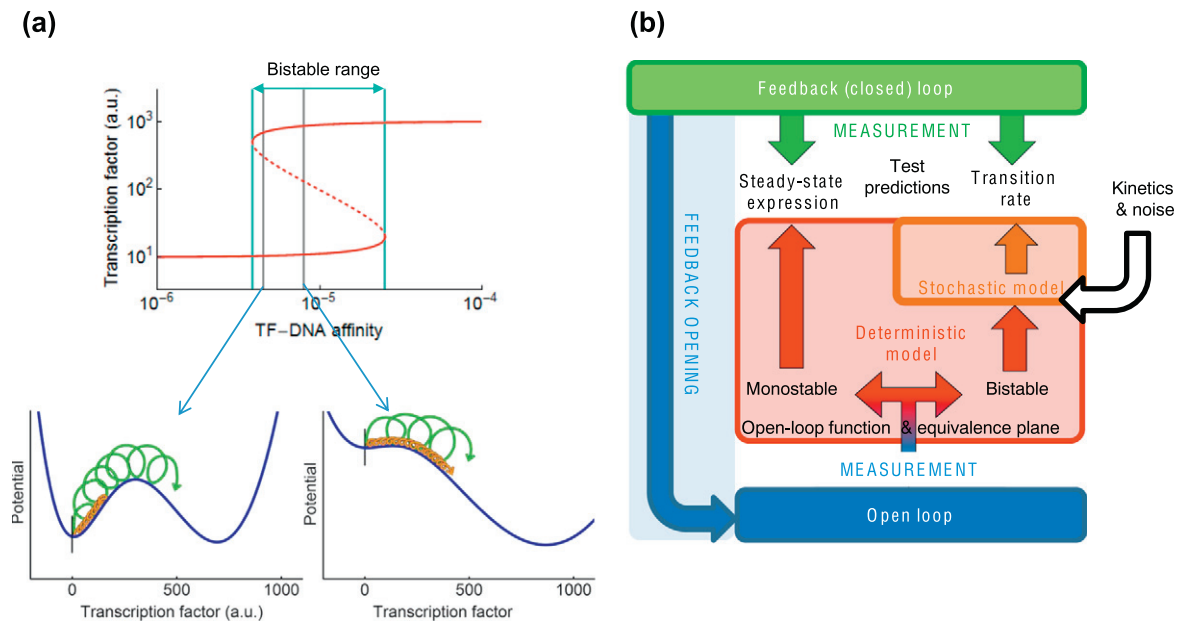


Fig. 1. Prediction of transition rates in bistable feedback loops. (a) A positive feedback loop displays bistability in a certain range of TF-DNA affinities. The two stable states correspond to potential wells. At higher TF-DNA affinity, the lower potential well becomes shallower (right panel) and the cells can more easily switch to the high state. The frequency of the transition is also influenced by noise intensity: weak noise (orange) and strong noise (green). (b) Prediction of transition rates and steady-state expression by feedback opening. The feedback loop is opened experimentally. The resulting open-loop function and the equivalence plane constitute a simple deterministic model. If they have a single intersection, the parent feedback is monostable. In this case, the intersection, which we termed open-to-closed loop mapping, can be directly compared to the measured steady-state expression in the feedback loop. If the parent feedback is classified as bistable, the open-loop function must be extended to a model by fitting the parameters to kinetic and noise measurements. The resulting stochastic model predicts the transition rates. The predictions are verified by measuring the feedback loop.

of the rates difficult. A possible way to predict the transitions is to measure individual reactions *in vitro* or *in vivo* and to combine all the reaction parameters into a model. However, many parameters in a circuit are experimentally inaccessible; their reported values can also scatter broadly, which hampers the prediction [11,12].

Here, we opted for a different approach comprising two stages. First, we employed a method termed feedback opening [13]. We opened synthetic feedback loops in the yeast *Saccharomyces cerevisiae*. Synthetic circuits have been playing an important role to characterize the fundamental properties of feedback behavior [14–18]. In the open loop, bistability is eliminated, and noise-induced transitions are bypassed. Therefore, we can obtain an open-loop function (f_{OLM}), which is the total response of all the reaction steps in the loop, without the need to resolve any of them individually. Since the f_{OLM} contains all the information on the deterministic steady-state expression, it can be used to determine if the parent closed (feedback) loop is bistable or monostable (Fig. 1b, deterministic model). In the second stage, we measured noise and the time scale of reactions, and by reintroducing noise into the model, we successfully predicted the transition rates (Fig. 1b, stochastic model).

Results

Design of the input and output constructs for the loop opening

To open a feedback loop, one of its components has to be split into an input and an output [13]. The resulting open loop is thus a reaction chain starting with the independently controllable input that triggers the biochemical reactions; the chain ends with the output, which has no effect on the reaction chain (Fig. 2a).

We opened transcriptional feedback loops at the RNA level in yeast (gray box, Fig. 2a), and thus, both the input and output are RNA molecules. The expressed input RNA is translated, which triggers the subsequent reactions, such as the transcription factor (TF) dimerization, the binding of the TF to the promoter, and lastly, the synthesis of the output RNA. The reactions between the input and output RNA are illustrated as a black box in Fig. 2a.

The input RNA is identical to the original RNA in the feedback loop. On the other hand, the output RNA has to be designed by mutating the original RNA. The mutation has to meet two requirements. First, the protein translated from the output mRNA must not interfere with the reactions in the loop

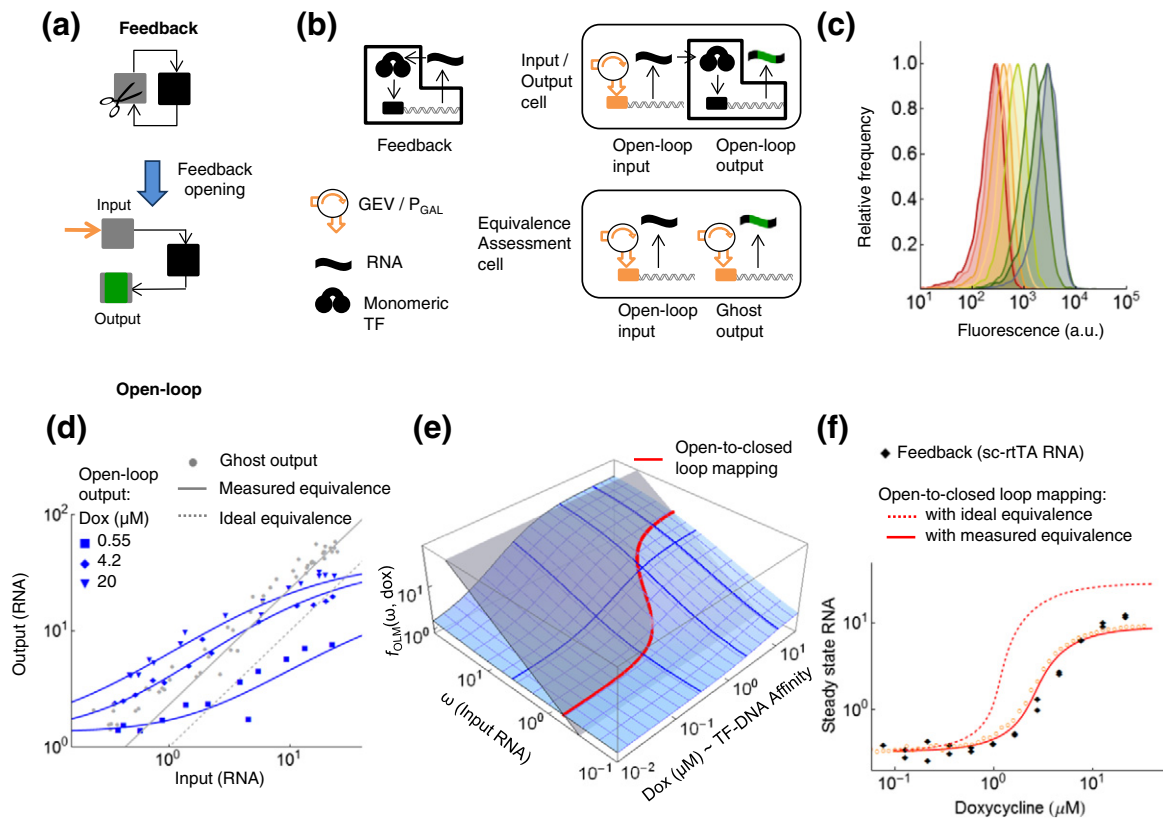


Fig. 2. Opening of the monomeric–noncooperative feedback loop ($P_{[\text{tetO}]1}$ -sc-rTA) classifies the parent loop as monostable. (a) To open a feedback loop, a component is chosen to be broken into an input and output. (b) The green segment in the output represents a heterologous sequence inserted for the feedback opening. (c) GFP fluorescence distribution in an open-loop-like construct, which contains a GFP reporter gene downstream of a $[\text{tetO}]1$ promoter controlled by sc-rTA. Cells were exposed to a gradient of dox concentrations (0.07, 0.12, 0.20, 0.33, 0.55, 0.91, 1.52, and 2.53 μM). (d) Open-loop measurements. The input and output RNA is measured, as the activity of the GAL promoter was varied by estradiol (see [Materials and Methods](#)) at three different fixed values of dox. (e) The measured equivalence (gray) and open-loop (blue) functions fitted to data shown in (d). The traces of the function denoted by blue thick lines correspond to the dox and estradiol concentrations used in the experiments (see also Fig. S3a). (f) Comparison of the open-to-closed loop mapping (red lines) with the steady-state expression measured for the feedback loop. The predicted mean steady state values from the stochastic simulation using the extended and fitted noise model are shown by orange circles.

(Fig. S1a). Second, the output RNA must preserve the original properties of the RNA, such as the decay rate and dynamic range of expression. We found that retaining only 45-bp long sequences at each end of a gene was sufficient to preserve much of the original expression range (Fig. S1b; Design of the output construct in the [Materials and Methods](#)). Therefore, we used this strategy to build the output construct (Fig. 2b). Since we used the TF rTA (reverse tetracycline transactivator) in the feedback loops, we built an output construct for rTA and tested for interference. The protein translated from such an output rRNA contains only short peptide sequences from rTA (15 aa at each end) and is unlikely to interfere with the reactions in the loop, which we confirmed experimentally (Fig. S1c–e).

By creating the input and the output constructs with the aforementioned method, the feedback is opened. The cells containing the open-loop input and output constructs were named Input/Output cells (Fig. 2b).

Validation of the loop opening with a monostable feedback loop

We opened three synthetic transcriptional feedback loops, in which a monomeric or dimeric version of the synthetic TF rTA regulates its own expression. rTA binds to the DNA when it is complexed with the ligand, doxycycline (dox) [19]. These feedback loops contained one (cooperative binding), two (homodimerization and cooperative binding), or no reactions that can support bistability [20]. First, we opened the

monomeric–noncooperative loop, in which a monomeric TF binds to a single binding site in its own promoter. The monomeric protein is a single-chain fusion of the dimeric rTA [20].

Upon opening this loop, the input and output RNAs were quantified by qPCR (quantitative PCR; Materials and Methods; Figs. 2, S2, and S3a). Thus, RNA values represent the averages of a cell population. The expression of the input was varied by tuning the P_{GAL} promoter activity with the TF GEV (Gal4-estrogen receptor-Vp16, Fig. 2d). We applied different concentrations of dox to adjust the TF-DNA binding affinity. Subsequently, we fitted an open-loop function, $\eta = f_{OLM}(\omega, dox)$, to these data. η , ω , and f_{OLM} denote the output, the input, and the open-loop function fitted to the measured data, respectively.

Initially, we analyzed the logarithmic sensitivity (S) of the f_{OLM} with respect to the input (ω), $S(\omega) = \partial \ln(f_{OLM}) / \partial \ln(\omega)$. If $S > 1$, the feedback loop can display bistability [21]. It is monostable if $S \leq 1$. $S(\omega)$ of the fitted $f_{OLM}(\omega, dox)$ did not exceed one at any value of ω and dox (Supplementary Information, Fitted open-loop functions). Thus, the monomeric–noncooperative feedback is classified as monostable upon the opening. This is in agreement with the expectations since the feedback does not contain any known reaction that can support bistability.

The intersection points of the f_{OLM} and the equivalence function (f_{EQ}) define the steady-state expression for the feedback loop [13,22]. The ideal f_{EQ} is an identity function, that is, it is the line at which the output and input have equal values, $\eta = \omega$ (Fig. 2d). The ideal equivalence assumes that the output and input RNAs have identical properties (expression range, synthesis, and decay rate). However, the heterologous sequence in the output RNA may cause a departure from the ideal equivalence. To

assess this departure, we expressed the input and output mRNAs under the control of identical promoter, P_{GAL} . The expression of the output RNA in this construct is not controlled by the input; therefore, we termed it ghost output (Fig. 2b). Although their decay rates of the mRNAs were similar (Fig. S2a and b), their expression levels differed (Fig. S2c–e), possibly because of the different RNA synthesis rates. There was a linear relationship between their expression levels with a non-unity slope (Fig. 2d). This slope defines the scaling factor (s) for the measured (nonideal) equivalence line, which runs in parallel to the ideal equivalence line (Fig. 2d): $f_{EQ}(\omega) = s\omega$.

The intersection of the measured f_{EQ} and f_{OLM} is a function of one variable (dox), which we termed open-to-closed loop mapping since it determines the steady-state expression in the closed feedback loop based on open-loop measurements (Fig. 2e and f, red full line). Importantly, there was a good agreement between the open-to-closed loop mapping and the steady-state expression measured in the feedback loop. If we had relied on the ideal equivalence plane, with a unity slope, the open-to-closed loop mapping would have deviated markedly from the values measured in the feedback loop (Fig. 2f, red dashed line). This underscores the importance of the equivalence assessment cells.

In summary, we validated the feedback opening in two main steps. First, we analyzed the open-loop constructs. The expression of a fluorescent reporter in open-loop-like constructs displays a unimodal distribution (Fig. 2c). The S of the f_{OLM} is less than one, which implies that the parent feedback loop is monostable. Since there are no noise-induced transitions between two stable states in a monostable feedback loop, the deterministic and stochastic descriptions of the steady-state expression levels

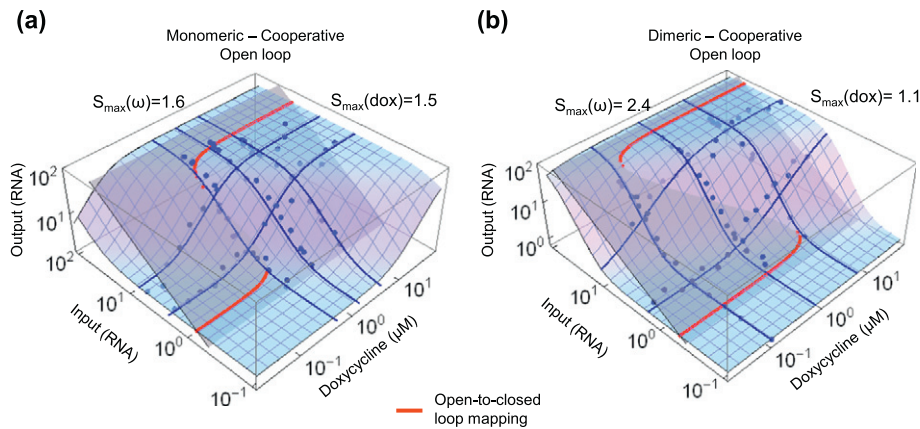


Fig. 3. Intersection of equivalence plane and f_{OLM} classifies two parent feedback loops as bistable. The blue and gray surfaces stand for the fitted f_{OLM} and the measured equivalence plane, respectively, fitted to experimental data (dots). The red curve is their intersection, the open-to-closed loop mapping. The maximal values of the S are calculated for the f_{OLM} with $b = 0.01 V_{max}$ by fixing either dox or ω . (a) Open-loop measurements of the $P_{[tetO]7}$ -sc-rTA circuit; $S_{max}(\omega, dox = 1.37) = 1.6$; $S_{max}(\omega = 2.11, dox) = 1.6$. (b) Open-loop measurements of the $P_{[tetO]7}$ -rTA circuit; $S_{max}(\omega, dox = 0.91) = 2.4$; $S_{max}(\omega = 1.93, dox) = 1.1$.

are expected to be similar. Consequently, the steady-state expression measured in the feedback loop can be directly compared to the value determined by feedback opening (Fig. 1b), provided that some general conditions are met (see Discussion). In the second step, we compared these two values. We found that the open-to-closed loop mapping matched up with the steady-state expression level measured in the feedback loop (Fig. 2f). The expression increased continuously and steeply when the TF-DNA affinity (i.e., dox concentration) passes a certain value, which is a typical behavior of monostable positive feedback loops.

Identification of bistability by loop opening

Next, we opened the loops with cooperative promoters, controlled by either the monomeric (Fig. 3a) or the dimeric TF (Fig. 3b). The sensitivity of $f_{\text{OLM}}(\omega, \text{dox})$ with respect to the input (ω) was higher than one for both open loops, which indicates that the feedback loop is bistable. Indeed, there was a range of dox concentration, at which the intersection

of the f_{OLM} with the equivalence plane resulted in three, (two stable and one unstable) steady state. Thus, both parent feedback loops are classified bistable.

The maximal sensitivity of the f_{OLM} , $S_{\text{max}}(\omega)$, has a major impact on the bistable range of a parameter. For the monomeric-cooperative circuit, $S_{\text{max}}(\omega)$ is 1.6. This value increased to 2.4 for the dimeric-cooperative circuit (Fig. 3b), and the bistable range of the dox concentration (i.e., TF-DNA affinity) became broader, reflecting the joint effect of dimerization and cooperativity (Fig. 3).

Measurement of the time scale of reactions and identification of the slow transient kinetics

To predict the transition rates for a bistable system, we have to combine the f_{OLM} , which is defined in the steady state, with information on noise and the time scale of reactions (Fig. 1b). To specify the time scale of reactions, we determined the RNA and protein decay rates and the transcription and translation rates (Table S2). With these parameters,

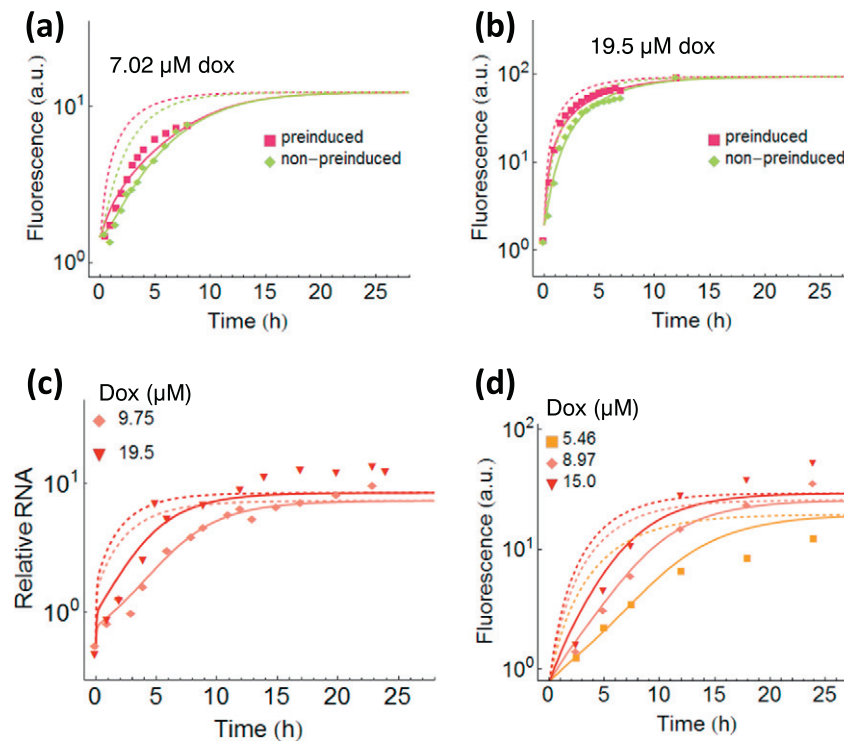


Fig. 4. Long transient phase upon the addition of dox to the cells. The curves represent the solution of the model without (dashed line) and with (full line) the extension to fit the transient kinetics. Dox was added at the indicated concentration at $t = 0$ h. (a and b) Induction kinetics in open-loop-like constructs, in which sc-rTA activates the expression of $P_{[\text{tetO}]2}$ -GFP (see transient kinetics strain in Table S1). The expression of sc-rTA was either pre-induced by estradiol (red) or induced at $t = 0$ h together with the addition of dox (green). Expression of GFP was measured with flow cytometry. To reach intermediate expression levels of sc-rTA, we applied 0.8 (a) and 7.28 (b) nM estradiol. (c and d) Induction kinetics of the monomeric-noncooperative feedback loop ($P_{[\text{tetO}]1}$ -sc-rTA). To report the feedback activity, we measured the mRNA of the sc-rTA (c) or the GFP expression driven by sc-rTA (d).

we extended the f_{OLM} into a kinetic model. We tested whether this model predicts correctly the kinetics of expression in open-loop-like constructs. For this purpose, we analyzed the time course of expression of green fluorescent protein (GFP) under the control of the monomeric form of rTA. Interestingly, the induction of expression was slower than expected from the time scales of protein and RNA turnover (Fig. 4a and b; see Modeling transient kinetics in the Supplementary Information). By varying the order of induction of the rTA expression and dox addition, it became clear that the slower-than-expected increase of GFP expression persisted even if rTA was pre-expressed (Fig. 4a and b). This indicates that the long transient phase arises due to the slow transport of the externally added ligand, dox, into the cell or due to its slow association with the protein inside the cell. The model was extended and fitted to the slow transient kinetics in the open-loop-like construct. Subsequently, we tested the prediction of the new model on the monostable feedback loop, which can be done deterministically. The prediction was in good agreement with the observed time series upon the addition of dox (Fig. 4c and d).

Measurement of noise

We made a preliminary prediction of noise intensity based on the time scale of the constitutive processes (mRNA and protein turnover). A simple model involving only synthesis and decay, also known as birth–death process, results in a Poisson distribution, characterized by a Fano factor (variance/mean) = 1 [23]. Interestingly, the housekeeping gene *PRE2*, which was used as a control for the single-molecule fluorescence in situ hybridization (smFISH), had a Fano factor close to 1 (Fig. 5a and b). On the other hand, the distribution of the rTA RNA had a much larger variance, with a Fano factor of around 5, which cannot be explained by such a simple noise model (Fig. 5a and b). This stronger noise is not fully surprising because noise in gene expression can be significantly augmented by operator fluctuations and by other cellular processes [24,25]. Therefore, the model was extended to include operator fluctuations and noise in RNA degradation (Fig. 5c). The parameters were fitted to the smFISH measurements (Supplementary Information, Determination of parameter values for RNA distribution by linear noise approximation), and the new extended and fitted model was in good agreement with the measured RNA distribution (Fig. 5a and b).

Comparison of deterministic and stochastic descriptions of the f_{OLM}

The open-loop function is a deterministic concept and can be considered to be a steady-state solution of ordinary differential equations. To predict the

transition rates, the deterministic model has to be converted to a stochastic one (Fig. 1b). This conversion is accurate, provided that the stochastic model of the open-loop function yields a mean value that is identical or similar to the deterministic value. The two values are identical, for example, for the mRNA birth–death process (Fig. 5a and b, see *PRE2*). However, this correspondence between the deterministic and stochastic models may be lost when the system is strongly nonlinear and the noise is large [26,27]. Such an effect was observed for a TF that displays stochastic nucleocytoplasmic shuttling [28].

We examined the effect of noise on the dimeric–cooperative open loop as it displays the response with the largest S in this study, and therefore, it is highly nonlinear. To explore how much noise shifts the value of the output mRNA, we performed stochastic simulation with the extended and fitted noise model. It yielded mean output RNA similar to the value of the deterministic function, f_{OLM} (Fig. 5d). This demonstrates that the effect of noise on this nonlinear f_{OLM} is negligible and the function can be used for accurate predictions. Thus, the loop opening bypasses the effect of noise. We also confirmed that gene expression in the open loop reaches a steady state after 24 h, independent of the initial condition, that is, it does not display hysteresis (Fig. S4). Furthermore, the distribution of gene expression in the corresponding open-loop-like constructs was unimodal (Fig. S3c).

Interestingly, there was also a good match between the (deterministic) open-to-closed loop mapping and the stochastic model of the monostable feedback loop (Fig. 2f, orange circles), which reveals that even the closed-loop response can have very similar stochastic and deterministic descriptions, provided it is monostable.

The predicted transition rates agree with the measurements

Upon extending the f_{OLM} using the reaction time scales and fitted noise, we reclosed the loop to predict the transition rates, both from the low to the high state and also in the opposite direction (high to low) for the two bistable circuits (Fig. 6). We also calculated the transition rates with the model not fitted to noise and transient kinetics for comparison. The simple noise model, characterized by smaller noise intensity, yielded slower transitions in the bistable range than the fitted, extended noise model (Fig. 6a–g). On the other hand, the transient kinetics reduced the transition rates only outside but not inside of the bistable range (Fig. 6b), exactly opposite to the effect of noise.

To test the predictions experimentally, we prepared pre-cultures with either low or high TF expression states, which define the initial condition, to measure how quickly they switch to the other

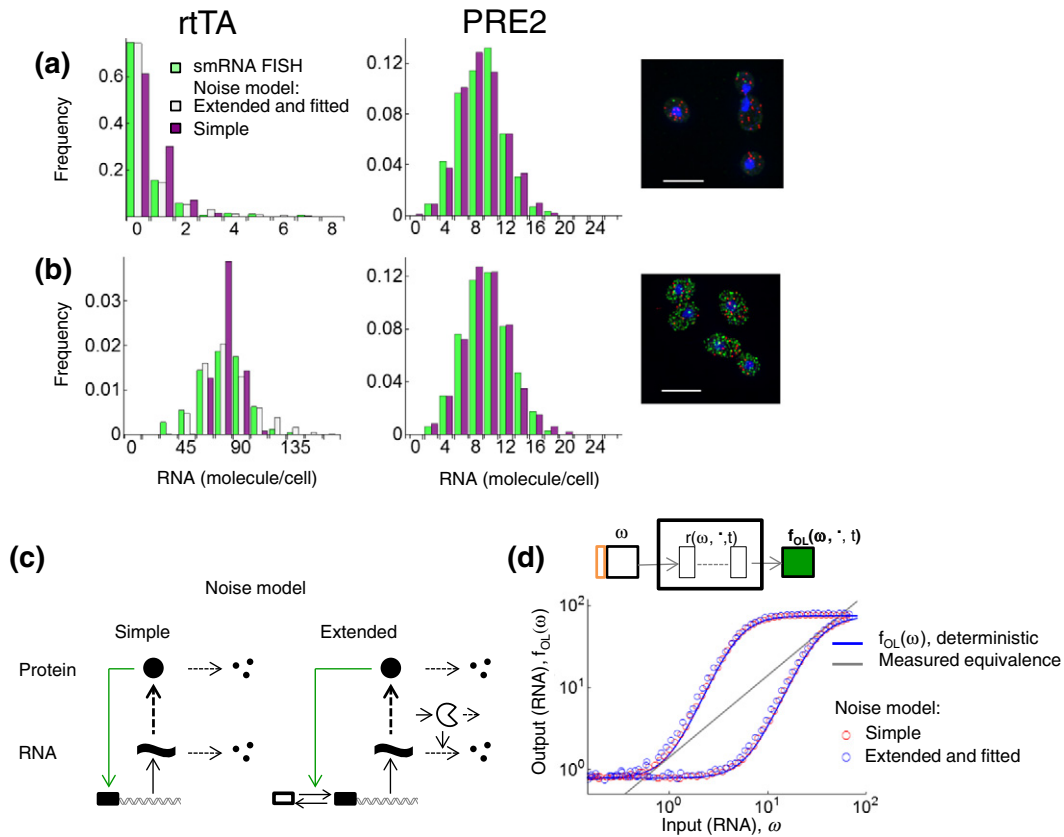


Fig. 5. Extension of the model to fit the measured noise. (a and b) FISH images and distributions of rTA and PRE2 RNA molecules in cells containing the $P_{[tetO]7}$ -rTA feedback loop either uninduced (a) or induced with $19.5 \mu\text{M}$ dox for 24 h in cultures with the high initial condition (b). We calculated the mean (molecules/cell), coefficient of variation (CV), and the Fano-factor (FF) for the measured distribution (subscript M) and the distribution simulated ($n = 1000$) with the simple (subscript S) or the extended and fitted noise model (subscript E ; see Mathematical modeling, simple and extended noise model). (a) The un-induced cells. For rTA: mean = 0.49; $CV_M = 2.31$; $FF_M = 2.41$ (green, $n = 280$); $CV_S = 1.46$; $CV_E = 2.22$. For PRE2: mean = 9.2; $CV_M = 0.32$; $FF_M = 0.94$; $CV_S = 0.33$. (b) The induced cells. For rTA: mean = 82.6; $CV_M = 0.24$; $FF_M = 4.80$ (green, $n = 171$); $CV_S = 0.11$; $CV_E = 0.26$. For PRE2: mean = 10.0; $CV_M = 0.31$; $FF_M = 0.98$; $CV_S = 0.32$. The images were obtained by z-projection of decomposed image stack of smFISH with the following coloring: blue, DAPI; green, rTA; red, PRE2; scale bar: $5 \mu\text{m}$. (c) To obtain a model that fits the experimental RNA distribution, the simple model is extended by operator fluctuation (forward and backward arrows) and enzymatic RNA degradation (Pac-Man). The thick dashed arrows indicate the step that is broken to open the feedback loop. (d) Comparison of the output RNA calculated by deterministic and stochastic models. To convert $f_{OLM}(\omega)$ into a model, reactions (r), were specified, which introduce time-dependent variables and parameters (denoted: \bullet). The steady-state solution of the deterministic model recreates the original $f_{OLM}(\omega)$. The mean RNA values were calculated by the simulation of the corresponding stochastic model (see Mathematical modeling, Conversion of the $f_{OLM}(\omega)$ to a reaction model). $f_{OLM}(\omega)$ corresponds to the thick curves at dox = 0.12 and $7 \mu\text{M}$ in Fig. 3b.

state. In the bistable range, the observed transition rates were in good agreement with the predictions using the fitted noise (Fig. 6b and g). Outside of the bistable range, the model with the fitted transient kinetics predicted well the observations (Fig. 6b). These results and the model predictions reveal that noise is the main determinant of transitions inside the bistable range, while transient kinetics is the main determinant of the transitions outside of the bistable range. It is important to reiterate that the transition rates were predicted without choosing or fitting parameter values to the observed transition rates.

For the dimeric-cooperative circuit, transitions from the low to the high state were only observed close to the bistability boundary at the higher dox concentration (Fig. 6g). Opposite transitions were observed close to the lower bistability boundary. Thus, there is a broad range of dox concentrations at which essentially no transitions are expected to occur between the two states. This range is positioned in the middle of the bistable range, determined by the open-to-closed loop mapping. Indeed, we have not observed any transition in this range of dox concentration even after 10 days (Fig. 6h).

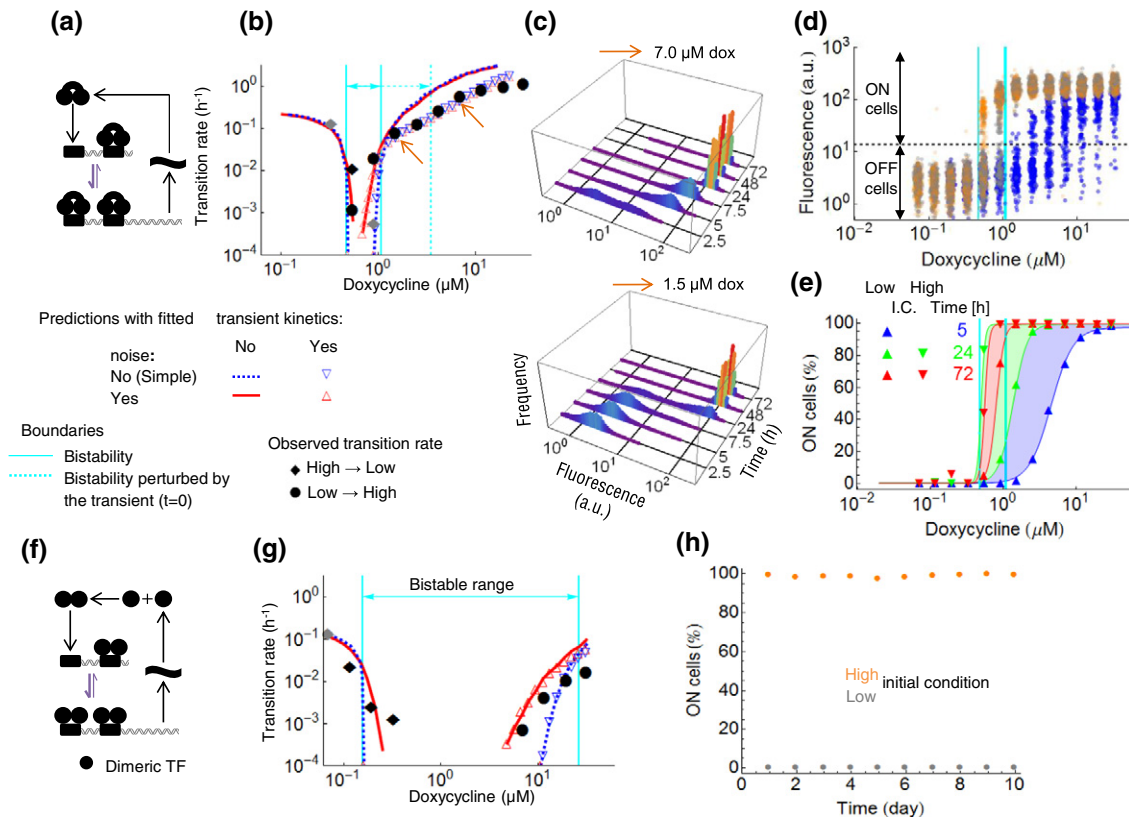


Fig. 6. Predicted and measured transition rates for the bistable, the monomeric-cooperative ($P_{[\text{tetO}]}7\text{-sc-rTA}$), (a–e) and the dimeric-cooperative ($P_{[\text{tetO}]}7\text{-rTA}$) (f–h) feedback loops. (a) Scheme of the feedback loop. (b) The orange arrows indicate the dox concentrations for which the time evolution of the fluorescence histograms is shown (in c). The gray symbols denote transition rates at the detection limit (see [Materials and Methods](#), Fitting of transition rates). (c) Fluorescence histograms of cells with the low initial condition. (d) Measurement of hysteresis experiments. Cells with low (gray dots) or high (orange dots) initial condition (I.C.) were grown for 72 h; 5 h measurements are shown only for the low I.C. (blue). (e) Measurement of hysteresis expressed in terms of ON cell percentages. Data are shown for cultures 5 h, 24 h, and 72 h after setting the initial condition. Identical to those shown in (d) are the 5 h and 72 h. The 24 h data are in Ref. [20]. (f) Scheme of the feedback loop. (g) Comparison of the measured and predicted transition rate for the dimeric-cooperative feedback loop. (h) Long-term hysteresis experiment with cells exposed to 0.92 μM dox.

For the monomeric-cooperative circuit, transitions were detected in both directions in the bistable range (Fig. 6b). Thus, equilibrium is expected to ensue in an experimentally realistic time scale. This can be visualized by plotting the experimental data in terms of hysteresis profiles, which is typically used to assess bistability, directly in feedback loops. For both initial conditions, we plotted the percentage of ON cells, that is, the proportion of cells in the high state (Fig. 6d and e). The range of dox concentrations at which the ON cell percentage in each culture remains close to the respective initial condition defines the hysteresis range. These two distinct expression states (OFF and ON cells) represent two “synthetic” cell fates. Interestingly, the hysteresis range changed with time for the monomeric-cooperative feedback loop (Fig. 6e). At early time points (5 h), the hysteresis range was broader than the bistability range (Fig. 6e). At a later time point

(72 h), the hysteresis nearly collapsed. This also implies that in noisy systems, hysteresis experiments may fail to distinguish bistable feedback loops from monostable ones after long periods of time.

Appearance of bimodality far away from the bistable range

When noise induces transitions between two stable states, both states become populated, resulting in a bimodal distribution. That is why bimodality is considered as a hallmark of bistability in noisy systems. However, it was surprising to observe that the transitions are accompanied with a bimodal distribution of GFP expression well beyond the bistable range for the monomeric-cooperative circuit (Fig. 6b and c). The range of this bimodality was around three times broader than the bistable range. We expected that the transient kinetics may be responsible for the

extension of the bimodality range because it prolongs the phase during which the TF-DNA affinity is approaching the final value upon the addition of dox to the cells (Fig. 6b, cyan dashed line), and it is this affinity that determines the bistability boundary. To visualize this, we superimposed single-cell trajectories of stochastic simulations onto a steady-state manifold perturbed by the transient kinetics. This manifold reflects the temporal changes in the bistability (Fig. 7, green surface). Initially, only few cells cross the unstable part of the manifold because it is far above the low expression state. As time progresses, the transient effect peters and the manifold recedes; the majority of cells transit as soon as the lower fold in the manifold crosses the dox concentration to which the cells are exposed. This explains how transient kinetics can slow down the transition rates and why bimodality, a sign of bistability, appears far away from the bistable range.

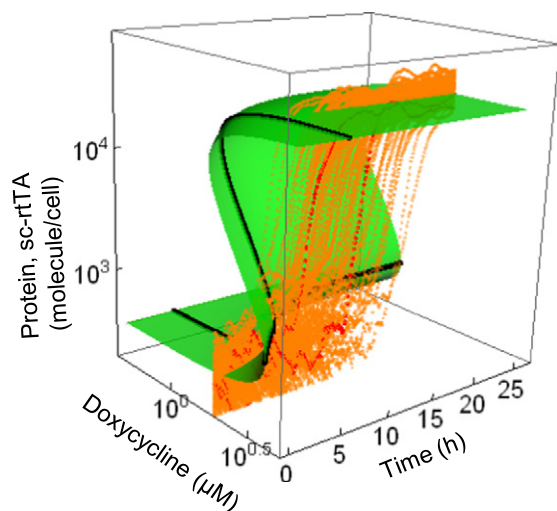


Fig. 7. Visualization of the effect of transient kinetics on the transitions. The parameter values for the monomeric-cooperative feedback loop were used for the simulation. The steady-state manifold (green surface) is perturbed by the transient kinetics to represent the temporal evolution of the TF-DNA affinity due to the slow effect of the externally added dox. Individual trajectories of stochastic simulations (with the model extended to fit noise and transient kinetics) are shown in orange and red. The horizontal black curve represents the evolution of the perturbed fold bifurcation point. The vertical black curve indicates the manifold at the time when the fold point passes the dox concentration that was used for the stochastic simulation (dox = 1.8 μM).

Discussion

Relation between bistability, bimodality, and hysteresis

Bimodality has been viewed as a sign of bistability, and hysteresis as the proof of bistability [29]. Our results reveal that neither hysteresis experiments nor bimodality can delimit the bistable range in noisy gene circuits. The hysteresis range shrinks with time (Fig. 6e) due to the noise-induced transitions and can even collapse in feedback loops that have a narrow bistable range. While hysteresis range may coincide with the bistable range at a particular time point, the length of this period is likely to vary from system to system. Bimodality, a potential sign of bistability, appeared far away from the bistable range due to the slow transient kinetics (Fig. 6b and c). Indeed, an increasing number of models have been identified, where bimodality appears without bistability or even in the absence of feedback regulation [30–33].

Since feedback opening bypasses noise, the open-to-closed loop mapping can determine whether a system is monostable or bistable and can delimit the bistable range.

Prediction of transition rates by feedback opening

Traditional modeling requires parameters for all reactions that comprise the feedback loop. However, models retain unidentified components, mechanisms, and parameters even after detailed measurements. In particular, binding constants are often missing or are inconsistent. For example, reported values for the dissociation equilibrium constants of the tetR-tet operator scatter over 3 orders of magnitude [11], which is relevant for rtTA, being a fusion protein of tetR. Furthermore, parameter values measured *in vitro* may significantly deviate from their values *in vivo* [12,34]. Therefore, several parameters are left free and then directly fitted to the transition rates, which makes true prediction impossible.

To predict the transition rates, we employed an inverse approach. By opening the feedback loop, we obtained an open-loop function, which lumps the steady-state response of all reactions in the feedback loop but does not resolve the time scale of any of them. To extend this function into a model, we performed kinetic and noise measurements. This extension has to be performed in a way that the model recreates the original steady state open-loop function (Fig. 5d, diagram). Not all reactions in the loop have to be identified. After measuring the core constitutive processes, including mRNA and protein turnover, we extended the model with a few additional parameters to fit the noise in gene expression and the transient kinetics (Fig. 1b). This was sufficient to

successfully predict the transition rates. We expect that, in general, it will be important to characterize the slow reactions (e.g., protein decay rate), since fast reactions (e.g., phosphorylation and dephosphorylation) are expected to be in equilibrium relative to the slow reactions.

The success of this approach may lie also in the fact that the initial steps of modeling were performed deterministically, which is typically more robust than the direct stochastic modeling of the whole feedback system [35,36].

Noise and bistability jointly determine transition rates

Inside the bistable range, the sensitivity of the f_{OLM} and noise are the key determinants of the transition rates. In the monomeric-cooperative loop, the $S_{\text{max}}(\omega)$ is 1.6. This value was 2.4 for the dimeric-cooperative loop, due to the dimerization. The system with higher sensitivity can be visualized by potential wells separated by higher barriers. This explains why the dimeric-cooperative loop is more stable than the monomeric-cooperative one: transi-

tions were too slow to be detected even after 10 days of incubation, that is, after more than 100 cell generations (Fig. 6h).

The open-to-closed loop mapping determines the steady-state expression levels and the bistable range of a parameter. Is this deterministic description relevant for bistable systems, knowing that it cannot be directly verified in noisy feedback loops? Our results indicate that the determination of the bistability boundaries permits targeted system identification (Fig. 8). Noise was the key determinant of the transitions inside the bistable range but not outside of it (Fig. 8, left). In this monostable range, we had to characterize transient kinetics to explain the transitions. The slow transient kinetics can be viewed as a temporal change in the potential barrier (Fig. 8, right).

The role of transient kinetics in cell fate transitions

When a parameter is in the monostable range in the vicinity of the bistable range, the slow transient kinetics is likely to be the rate-limiting step in the transitions. In such cases, the activity of the

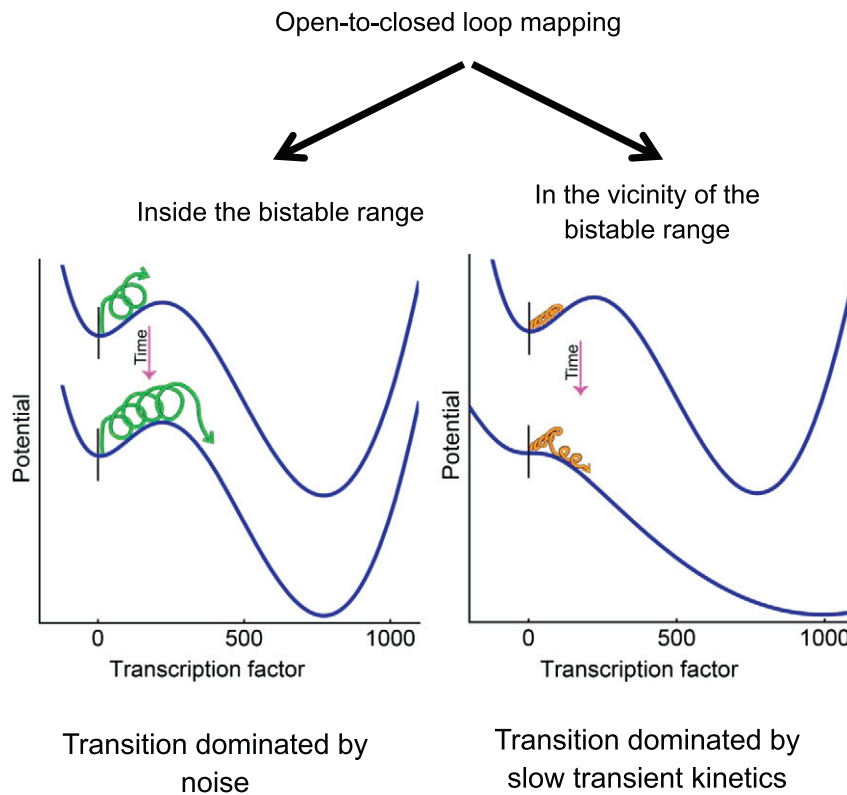


Fig. 8. The role of bistability, noise, and transient kinetics in the cell fate transitions. If a network displays steady-state bistability, as determined by feedback opening, the depth of the potential wells and noise are the main determinants of the transition rate (left). If the parameters of the network are outside but in the vicinity of the bistable range, the transitions are determined by the long transient phase, which can arise due to slow transport, metabolism, or other deterministically described transient cellular process (right).

feedback loop is controlled by an extracellular factor that evokes slow changes in transport, metabolism, or signal transduction. The two distinct cell fates can be maintained only transiently. However, such a transient phenomenon may be of considerable utility, since an increasing number of studies revealed that alternative fates exist transiently in many cells and organisms [5,37–40]. It is possible that differentiation should be considered as series of transient events, and the steady state is reached only in the terminal stage [7]. Upon the completion of differentiation, only a true bistable state can warrant long-term stability. In this case, transitions will be induced by noise and exemplified by noise in gene expression. Such transitions can destabilize cell fates, which can hamper cellular reprogramming [6], but can also help adaptation by diversifying the phenotypes of immune cells to combat pathogens.

Validity of prediction by feedback opening

In this study, we opened simple positive feedback loops. Can we expect that the opening is a valid approach for more complex networks? Two aspects of the loop opening are particularly relevant to more complex networks: (1) the theorem that deduces the existence of bistability from open-loop properties and (2) the stochasticity in the open loop.

With respect to the first aspect, a general theorem states that if the open-loop function is sigmoidal (i.e., the open-loop function has an S higher than one) and satisfies some general conditions, the parent feedback loop is bistable, independent of the time scale of the reactions [13]. Positive feedback loops with cooperative binding and dimerization, which were used in our work, satisfy the general conditions. However, if a network contains also a negative feedback loop, bistability is not guaranteed. In such dual positive–negative feedback loops, the concentrations of the components may oscillate over time rather than converge to one of the stable states. In the experimental practice, however, such restrictions may be less severe as the feedback system can be directly measured whether it displays oscillations. If it does not oscillate but displays signs of bistability, bimodality, and hysteresis, it is likely that the open-loop function will correctly predict the existence of bistability, even if a more complex network contains a negative feedback loop.

The aforementioned theorem is defined in a deterministic framework. We are not aware of the theoretical studies that formulate the open-loop approach in a stochastic framework, which is relevant to noisy gene networks. Therefore, we performed the following tests to show that the

deterministic and stochastic descriptions of the open loop are similar. First, we showed that there is no hysteresis after 24 h in the open loop. Second, the distribution of gene expression is unimodal. Third, we compared the f_{OLM} , which is defined deterministically, to the mean value of the output calculated using the expanded model upon the identification of the time scale of the main reactions. The two values were similar, that is, there is no marked stochastic deviant effect [27]. Further studies will be needed to explore how the open-loop function is affected by noise in more complex networks.

Feedback opening and the subsequent model extension are expected to be useful to predict transition rates and identify the main determinants of cell fate transitions: bistability in the deterministic sense, noise, and transient kinetics. This distinction may also help in engineering cell fate transitions.

Materials and Methods

Design of synthetic circuits and yeast strains

Three major strain types were used in this study: the feedback, Input/Output, and Equivalence Assessment cells (Table S1). The feedback cells contained a feedback circuit, a fluorescent reporter construct ($P_{[tetO]_2^-}$ yEGFP), and a construct to adjust the high condition (P_{GAL^-} (sc-)rtTA), which is identical to the open-loop input construct.

The Input/Output cells contained the open-loop output, open-loop input constructs, and a constitutively expressed GEV. The Equivalence Assessment cells contained the ghost output (P_{GAL^-} (sc-)rtTA Δ (45/45)::yellow fluorescent protein), the open-loop input construct, and a constitutively expressed GEV. The expression of the open-loop input and ghost-output constructs was controlled by GEV. GEV is a transcription activator consisting of a Gal4p DNA-binding domain, an estradiol receptor, and a VP16 activation domain. RNA expression was tuned over a broad range by adding estradiol at a concentration between 0 and 200 nM [41].

Design of the output construct

The two requirements, lack of interference and preservation of expression properties, make opposing demands on the optimal scale of the mutation to construct the output. For example, if the output gene contains a minor (e.g., point) mutation in the DNA-binding domain of the TF, the properties of the encoding mRNAs are likely to be preserved, and the loop is successfully broken because the TF will not bind to the DNA. However, a TF with a minor mutation may still cross-dimerize with the wild-type TF translated from the input RNA, interfering with the signaling in the open loop. A large-scale mutation, whereby the entire coding region

is replaced by a heterologous sequence, eliminates the interference, but the dynamic range of the expression may be reduced. To find the maximal length of the replacement with a minimal effect on mRNA expression, we built a series of genetic replacement constructs by varying the length of the sequence retained from the original gene (Fig. S1a and b).

Construction of yeast strains

All yeast strains are derivatives of *S. cerevisiae* W303, except for the strains to test the expression range of *GAL2* gene as a function of the length of the replaced open reading frame (ORF). All genetic constructs were integrated into the chromosome with a single copy, with the exception of the GEV construct, which has around five copies, and the $P_{[\text{tetO}]2}$ -GFP construct, which has three copies.

The feedback, open-loop input, the open-loop output, and ghost output constructs share a common core promoter and transcriptional terminator of *CYC1*. The input and ghost output were controlled by the P_{GAL} , whereas the feedback and output constructs were controlled by $P_{[\text{tetO}]1}$ or $P_{[\text{tetO}]7}$ for noncooperative and cooperative binding, respectively. Into each feedback construct, an optimized stem-loop was inserted to avoid growth alterations [20]. The same stem-loop was also inserted in the corresponding open-loop input, open-loop output, and ghost output constructs.

To construct the open-loop output and ghost output constructs, we flanked the yellow fluorescent protein sequence with 45-bp sequences from both ends of the rTA ORF. The flanking sequences of sc-rTA and rTA ORFs are identical because sc-rTA was constructed by inserting humanized tetR sequence into the rTA sequence [20].

To minimize the position effect, we integrated the genes with promoters containing tet operators to the *ura3* locus and those with P_{GAL} to the *ade2* locus. Using diploid cells for the optimized constructs made it possible to have two constructs with the same promoter at the same locus, which is essential for constructing the Equivalence Assessment strains. In addition, the transformations followed the order of (1) GEV, (2) open-loop input, and then (3) open-loop output, ghost output, or feedback construct, in order to have identical sequence and copy number of GEV and open-loop input constructs between the different strains.

Growth conditions

Cultures were grown at 30 °C, and the OD_{600} was kept below 1.0; were refreshed by diluting the cultures twice a day. A sample was collected for measurement, and the cell density was between 0.6 and 1.0. For the steady-state RNA measurements, cultures were grown for 24 h. To set the initial condition in the feedback loops, we added 0.5% galactose to the medium to drive expression under the control of the P_{GAL} promoter through the endogenous Gal4p, as previously described [20].

To determine RNA decay rate constants, shutoff assays were performed. The cells were cultured overnight with 0.5% galactose and transferred to a refreshment medium containing 0.04% galactose for further

growth for 4 h. To shut off transcription, the cells were pelleted and cultured further in medium without galactose. As described, 5 ml culture was collected with dry ice-cooled methanol [41]. Decay rates were obtained by linear regression.

Flow cytometry [20] and beta-galactosidase assay [14] were performed as described previously.

RNA quantification

RNA was quantified with qPCR and smFISH as previously described [20]. The overall efficiency for the input primer pair, which was identical for both the rTA/sc-rTA primer pairs, was 1.931; the efficiency for the output primer pair (F: 5'-CGGGGGATCCATGCCTA-GATTA-3'; R: 5'-ACTGACAGAAAATTTGTGCCCAT-3') was 1.934. The forward primer sequence is identical for the input and the output.

Absolute quantification of cellular RNA molecules was performed by smFISH. The results from smFISH were utilized for assessing the noise in gene expression in the feedback strains and for converting the RNA quantified in qPCR to the absolute mRNA number in the cell. We obtained the constant ratio α (Supplementary Information, Scaling of output signal for fitted equivalence) by quantifying the RNA at high expression state with the dimeric-cooperative and monomeric-cooperative feedback strains with both qPCR and smFISH. In the indicated experimental conditions, all cells were *PRE2* positive with 10.51 ± 0.75 (mean \pm sd) RNA molecule per cell. The background level of rTA RNA (false positive) count was ~ 0.03 spots per cell, in cells without the rTA construct (Table S1, Ych294). The spot intensity distribution was unimodal, indicating that a single molecule was detected at each spot (Fig. S5) [42].

Fitting of transition rates

To fit transition rates with the low initial condition, samples were collected at 2.5, 5, 7.5, 24, 48, and 72 h. With the high initial condition, samples were collected at 24, 48, and 72 h; earlier time points were omitted because of the slow dilution of the GFP signal during cell division.

The ON and OFF cell population was separated by a threshold value. The threshold was set equal to the geometric mean of the maximally induced (at 19.5 μM dox) fluorescence intensity and the uninduced fluorescence intensity measured at 72 h.

At most dox concentrations, detectable transitions of sufficient rates occur only in one direction. In these cases, we obtained the best fits for the transition rates with data expressing OFF cell proportion (r) and with inverse-square (Y^{-2}) weighting. The low-to-high state transition was fitted with the low initial condition, $r(t) = e^{-k_{\text{up}}t}$, and the high-to-low state transition was fitted with the high initial condition, $r(t) = 1 - e^{-k_{\text{down}}t}$.

When the bistable range is narrow, transitions occur in both directions. Consequently, the percentage of OFF cells stays between 4% and 96% at 72 h. In these cases, we performed fitting with equations describing bidirectional transitions without weighting.

For the low initial condition:

$$r(t) = \frac{k_{\text{down}} + k_{\text{up}} e^{-(k_{\text{up}} + k_{\text{down}})t}}{k_{\text{up}} + k_{\text{down}}}$$

For the high initial condition:

$$r(t) = \frac{k_{\text{down}} - k_{\text{down}} e^{-(k_{\text{up}} + k_{\text{down}})t}}{k_{\text{up}} + k_{\text{down}}}$$

The values with the lower standard error were taken from the fitting.

Due to the fluctuations in conditions, we did not consider the data that were close to the detection limit of a change, less than 4% difference between $r(2.5 \text{ h})$ and $r(72 \text{ h})$. This imposes the upper and lower detection limit of transition rates. For the low initial condition experiments, the limits are $k_{\text{up}} = 1.3 \text{ h}^{-1}$, when $r(2.5 \text{ h}) = 0.04$; and $k_{\text{up}} = 5.6 \cdot 10^{-4} \text{ h}^{-1}$, when $r(72 \text{ h}) = 0.96$. A similar detection limit can be established for the reverse transition: $k_{\text{down}} = 0.13 \text{ h}^{-1}$, when $r(24 \text{ h}) = 0.96$; and $k_{\text{down}} = 5.6 \cdot 10^{-4} \text{ h}^{-1}$, when $r(72 \text{ h}) = 0.04$.

Acknowledgments

We thank Simone Scherrer for the help with plasmid and yeast construction for assessment of flanking region. This work was supported by grants from the Swiss National Foundation and the StoNets RTD from SystemsX. C.H. was a Long-Term Fellow of the Human Frontier Science Program.

Author contributions: A.B. designed the project. C.H. and V.J. did the experiments and data analysis. F.M., A.B., and C.H. did the modeling and simulations. A.B. and C.H. wrote the paper with input from all the authors.

Appendix A. Supplementary Data

Supplementary data to this article can be found online at <http://dx.doi.org/10.1016/j.jmb.2016.07.024>.

Received 24 June 2016;

Received in revised form 26 July 2016;

Accepted 29 July 2016

Available online 4 August 2016

Keywords:

positive feedback loop;
stochastic gene expression;
synthetic biology

†C.H. and V.J. contributed equally to this work.

Abbreviations used:

TF, transcription factor; dox, doxycycline; ORF, open reading frame; smFISH, single molecule fluorescence in

situ hybridization; S, logarithmic sensitivity; f_{OLM} , open-loop function; f_{EQ} , equivalence function; $S_{\text{max}}(\omega)$, maximal sensitivity of the f_{OLM} ; rTA, reverse tetracycline transactivator; GEV, Gal4-estrogen receptor-Vp16; GFP, green fluorescent protein; I.C., initial condition.

References

- [1] M. Arnoldini, I.A. Vizcarra, R. Pena-Miller, N. Stocker, M. Diard, V. Vogel, et al., Bistable expression of virulence genes in salmonella leads to the formation of an antibiotic-tolerant subpopulation, *PLoS Biol.* 12 (2014), e1001928 <http://dx.doi.org/10.1371/journal.pbio.1001928>.
- [2] G. Balazsi, A. van Oudenaarden, J.J. Collins, Cellular decision making and biological noise: from microbes to mammals, *Cell.* 144 (2011) 910–925.
- [3] D. Jukam, B. Xie, J. Rister, D. Terrell, M. Charlton-Perkins, D. Pistillo, et al., Opposite feedbacks in the Hippo pathway for growth control and neural fate, *Science.* 342 (2013) 1,238,016, <http://dx.doi.org/10.1126/science.1238016>.
- [4] M. Bednarz, J.A. Halliday, C. Herman, I. Golding, Revisiting bistability in the lysis/lysogeny circuit of bacteriophage lambda, *PLoS One.* 9 (2014), e100876 <http://dx.doi.org/10.1371/journal.pone.0100876>.
- [5] N. Mirouze, Y. Desai, A. Raj, D. Dubnau, Spo0A~P imposes a temporal gate for the bimodal expression of competence in *Bacillus subtilis*, *PLoS Genet.* 8 (2012), e1002586 <http://dx.doi.org/10.1371/journal.pgen.1002586>.
- [6] S. Pacini, Deterministic and stochastic approaches in the clinical application of mesenchymal stromal cells (MSCs), *Front. Cell Dev. Biol.* 2 (2014) 50, <http://dx.doi.org/10.3389/fcell.2014.00050>.
- [7] J. Ladewig, P. Koch, O. Brustle, Leveling Waddington: the emergence of direct programming and the loss of cell fate hierarchies, *Nat. Rev. Mol. Cell Biol.* 14 (2013) 225–236.
- [8] A.M. Walczak, J.N. Onuchic, P.G. Wolynes, Absolute rate theories of epigenetic stability, *Proc. Natl. Acad. Sci. U. S. A.* 102 (2005) 18,926–18,931.
- [9] J.X. Zhou, M.D. Aliyu, E. Aurell, S. Huang, Quasi-potential landscape in complex multi-stable systems, *J. R. Soc. Interface.* 9 (2012) 3539–3553.
- [10] P. Érdi, J. Tóth, *Mathematical Models of Chemical Reactions: Theory and Applications of Deterministic and Stochastic Models*, Princeton University Press, Princeton, N.J., 1989.
- [11] C. Berens, D. Porschke, Recognition of operator DNA by Tet repressor, *J. Phys. Chem. B* 117 (2013) 1880–1885.
- [12] R. Garcia-Contreras, P. Vos, H.V. Westerhoff, F.C. Boogerd, Why *in vivo* may not equal *in vitro*—new effectors revealed by measurement of enzymatic activities under the same *in vivo*-like assay conditions, *Febs J.* 279 (2012) 4145–4159.
- [13] D. Angeli, J.E. Ferrell Jr., E.D. Sontag, Detection of multistability, bifurcations, and hysteresis in a large class of biological positive-feedback systems, *Proc. Natl. Acad. Sci. U. S. A.* 101 (2004) 1822–1827.
- [14] C. Hsu, S. Scherrer, A. Buetti-Dinh, P. Ratna, J. Pizzolato, V. Jaquet, et al., Stochastic signalling rewires the interaction map of a multiple feedback network during yeast evolution, *Nat. Commun.* 3 (2012) 682, <http://dx.doi.org/10.1038/ncomms1687>.

- [15] Y.T. Maeda, M. Sano, Regulatory dynamics of synthetic gene networks with positive feedback, *J. Mol. Biol.* 359 (2006) 1107–1124.
- [16] M.C. Inniss, P.A. Silver, Building synthetic memory, *Curr. Biol.* 23 (2013) R812–R816.
- [17] K.C. Ma, S.D. Perli, T.K. Lu, Foundations and emerging paradigms for computing in living cells, *J. Mol. Biol.* 428 (2016) 893–915.
- [18] M. Wu, R.Q. Su, X. Li, T. Ellis, Y.C. Lai, X. Wang, Engineering of regulated stochastic cell fate determination, *Proc. Natl. Acad. Sci. U. S. A.* 110 (2013) 10,610–10,615.
- [19] A. Kamionka, M. Majewski, K. Roth, R. Bertram, C. Kraft, W. Hillen, Induction of single chain tetracycline repressor requires the binding of two inducers, *Nucleic Acids Res.* 34 (2006) 3834–3841.
- [20] C. Hsu, V. Jaquet, M. Gencoglu, A. Becskei, Protein dimerization generates bistability in positive feedback loops, *Cell Rep.* 16 (2016) 1204–1210.
- [21] I. Majer, A. Hajihosseini, A. Becskei, Identification of optimal parameter combinations for the emergence of bistability, *Phys. Biol.* 12 (2015) 066,011, <http://dx.doi.org/10.1088/1478-3975/12/6/066011>.
- [22] N. Rai, R. Anand, K. Ramkumar, V. Sreenivasan, S. Dabholkar, K.V. Venkatesh, et al., Prediction by promoter logic in bacterial quorum sensing, *PLoS Comput. Biol.* 8 (2012), e1002361 <http://dx.doi.org/10.1371/journal.pcbi.1002361>.
- [23] M. Thattai, A. van Oudenaarden, Intrinsic noise in gene regulatory networks, *Proc. Natl. Acad. Sci. U. S. A.* 98 (2001) 8614–8619.
- [24] A. Raj, C.S. Peskin, D. Tranchina, D.Y. Vargas, S. Tyagi, Stochastic mRNA synthesis in mammalian cells, *PLoS Biol.* 4 (2006), e309 <http://dx.doi.org/10.1371/journal.pbio.0040309>.
- [25] S. Tsuru, J. Ichinose, A. Kashiwagi, B.W. Ying, K. Kaneko, T. Yomo, Noisy cell growth rate leads to fluctuating protein concentration in bacteria, *Phys. Biol.* 6 (2009) 036015, <http://dx.doi.org/10.1088/1478-3975/6/3/036015>.
- [26] O.G. Berg, J. Paulsson, M. Ehrenberg, Fluctuations and quality of control in biological cells: zero-order ultrasensitivity reinvestigated, *Biophys. J.* 79 (2000) 1228–1236.
- [27] M.S. Samoilov, A.P. Arkin, Deviant effects in molecular reaction pathways, *Nat. Biotechnol.* 24 (2006) 1235–1240.
- [28] L. Cai, C.K. Dalal, M.B. Elowitz, Frequency-modulated nuclear localization bursts coordinate gene regulation, *Nature.* 455 (2008) 485–490.
- [29] A.J. Ninfa, A.E. Mayo, Hysteresis vs. graded responses: the connections make all the difference, *Sci. STKE* 2004 (2004), pe20 <http://dx.doi.org/10.1126/stke.2322004pe20>.
- [30] R. Hermesen, D.W. Erickson, T. Hwa, Speed, sensitivity, and bistability in auto-activating signaling circuits, *PLoS Comput. Biol.* 7 (2011), e1002265 <http://dx.doi.org/10.1371/journal.pcbi.1002265>.
- [31] A. Lipshtat, A. Loinger, N.Q. Balaban, O. Biham, Genetic toggle switch without cooperative binding, *Phys. Rev. Lett.* 96 (2006) 188,101, <http://dx.doi.org/10.1103/PhysRevLett.96.188101>.
- [32] A. Ochab-Marcinek, M. Tabaka, Bimodal gene expression in noncooperative regulatory systems, *Proc. Natl. Acad. Sci. U. S. A.* 107 (2010) 22,096–22,101.
- [33] T.L. To, N. Maheshri, Noise can induce bimodality in positive transcriptional feedback loops without bistability, *Science.* 327 (2010) 1142–1145.
- [34] C. Chen, R. Bundschuh, Quantitative models for accelerated protein dissociation from nucleosomal DNA, *Nucleic Acids Res.* 42 (2014) 9753–9760.
- [35] D.J. Wilkinson, Stochastic modelling for quantitative description of heterogeneous biological systems, *Nat. Rev. Genet.* 10 (2009) 122–133.
- [36] T. Gedeon, P. Bokes, Delayed protein synthesis reduces the correlation between mRNA and protein fluctuations, *Biophys. J.* 103 (2012) 377–385.
- [37] G. Yao, C. Tan, M. West, J.R. Nevins, L. You, Origin of bistability underlying mammalian cell cycle entry, *Mol. Syst. Biol.* 7 (2011) 485, <http://dx.doi.org/10.1038/msb.2011.19>.
- [38] J.W. Veening, O.A. Igoshin, R.T. Eijlander, R. Nijland, L.W. Hamoen, O.P. Kuipers, Transient heterogeneity in extracellular protease production by *Bacillus subtilis*, *Mol. Syst. Biol.* 4 (2008) 184.
- [39] L.S. Weinberger, R.D. Dar, M.L. Simpson, Transient-mediated fate determination in a transcriptional circuit of HIV, *Nat. Genet.* 40 (2008) 466–470.
- [40] G.M. Suel, J. Garcia-Ojalvo, L.M. Liberman, M.B. Elowitz, An excitable gene regulatory circuit induces transient cellular differentiation, *Nature.* 440 (2006) 545–550.
- [41] M.M. Bonde, S. Voegeli, A. Baudrimont, B. Seraphin, A. Becskei, Quantification of pre-mRNA escape rate and synergy in splicing, *Nucleic Acids Res.* 42 (2014) 12,847–12,860.
- [42] A. Raj, P. van den Bogaard, S.A. Rifkin, A. van Oudenaarden, S. Tyagi, Imaging individual mRNA molecules using multiple singly labeled probes, *Nat. Methods* 5 (2008) 877–879.